Hindawi Publishing Corporation
Advances in Civil Engineering
Volume 2010, Article ID 253274, 8 pages
doi:10.1155/2010/253274

Research Article

An FBG-Based Impact Event Detection System for Structural Health Monitoring

C. S. Shin,[1] B. L. Chen,[1] and S. K. Liaw[1,2]

[1] *Department of Mechanical Engineering, National Taiwan University, Taipei 10617, Taiwan*
[2] *Department of Electronic Engineering, National Taiwan University of Science and Technology, Taipei 106, Taiwan*

Correspondence should be addressed to C. S. Shin, csshin@ntu.edu.tw

Received 1 September 2009; Revised 5 December 2009; Accepted 26 January 2010

Academic Editor: Yi Qing Ni

Some structures are vulnerable to localized internal damages incurred by impact of small objects. An impact monitoring system using fiber Bragg grating (FBG) sensors has been established. Its ability to detect very low to medium energy impacts has been demonstrated on an aluminum plate and a 22 m long wind turbine blade. Previous analysis of this technique showed that the accuracy by which an impact position can be located is limited by equipment noises and angular insensitivity of the FBG. By employing two intensity demodulation schemes with different demodulation sensitivities and ranges, we try to differentiate the relative importance of the above limiting effects. Based on the results, directions for further improvement on impact source locating accuracy will be discussed and the implication of applying such systems on large-scale structures will be examined.

1. Introduction

Impacts due to bird-strike and hailstorm may do much harm to structures such as aircraft and wind turbine blades. The structure will be especially vulnerable if it is made of polymeric composite as impacts may induce localized small internal damages. On actingupon by fluctuating service loading, these insidious defects may grow and eventually lead to catastrophic failures. Although nondestructive examination techniques for the detection of internal damages are available, they are limited in resolution. Moreover, to stage a thorough examination over the entire structure can be highly time and resource consuming for a large-scale structure. The problem can be much alleviated if one knows where to look at and what to look for.

The current work investigates the possibility of establishing an impact event monitoring system using fiber Bragg grating (FBG). FBG has found increasing applications as sensors in aerospace, structural, medical, and chemical applications for vibration, temperature, strain, impact, and general structural health monitoring [1–5]. It is chosen in the current task because of its good long-term durability and stability. In case of composite structures, optical fiber sensors possess the additional advantage of being compatible with common polymeric materials, making them easily embeddable inside a structure without inducing significant weakening of the material.

Previous works on impact location identification mostly used piezoelectric sensors (e.g., [6, 7]). A three-sensor-based scheme was used to locate the impact position of a projectile on a target screen by measuring acoustic waves with microphones [8, 9]. However, this scheme requires *a priori* knowledge of the wave speed. For practical applications, calibration of the wave speed in advance may not be feasible. Our own work showed that the whereabouts of an impact event can be located by analyzing the differential time-of-flight among signals picked up by four different FBG sensors [10]. Changes in the measurand are reflected as shift in the characteristic Bragg wavelength of an FBG. Light intensity demodulation techniques [11–13] have been shown to possess the required dynamic response for logging impact events [10, 14, 15]. In this work, two different light intensity demodulation schemes have been compared. The possibility of logging and locating impact will be tested on a flat aluminum plate and a wind turbine blade.

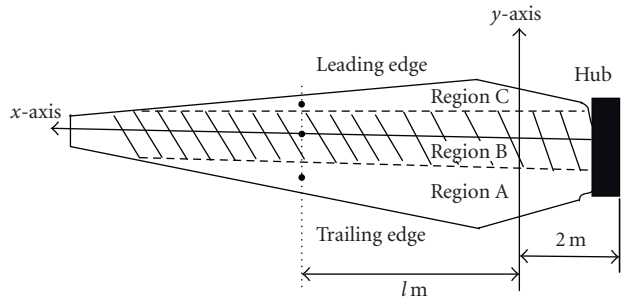

Figure 1: 2D Schematics of the blade (hatched area indicates region with interior box beam).

2. Experimental and Analysis Procedures

2.1. Impact Testing. Impact testing was made on a 0.8 m × 0.8 m square aluminum plate with a thickness of 6 mm and a retired 22 m long composite blade from a 660 kW wind turbine. The cross section of the blade essentially consists of an upper and lower aerodynamic surfaces with a reinforcing box beam sandwiched in between. Figure 1 shows a 2D schematics of the top surface of the blade. For convenience in the following description, the blade is divided into 3 regions. The hatched area, designated Region B, indicates the position of the box beam. Regions A and C are, respectively, the trailing and leading edges of the blade. The longitudinal mid-axis of the beam is taken as the x-axis. The corresponding y-axis is situated 2 m from the hub base. Sensing FBGs oriented along the x direction were stuck on the y-axis at the center of each of the three regions. Impact events were generated using a Bruel & Kjaer Type 8202 hammer at various distances l m from the y-axis. At any section, impact was made at the center of a region (the dots in Figure 1). For the aluminum plate, impacts were made by dropping a 70 g aluminum projectile from various heights H. For impact source locating, impacts from $H = 15$ cm were made on a grid at 10 cm increment along the horizontal and vertical directions. Because of symmetry, impacts were made only on half of the plate. Location of the sensing FBGs on the plate will be described in a latter section. All FBGs used in the current work were fabricated by side writing on single mode photosensitive fibers. The reflectivity of the FBG was about 99%, with the peak wavelengths between 1551 nm and 1552 nm. The shift of the peak wavelength caused by transient stress waves was interrogated with two different intensity demodulation schemes.

2.2. FBG Interrogating Schemes. Figure 2 shows the two light intensity demodulation schemes employed. For the one involving an ASE light source (Figure 2(a)), a commercial edge filter (Santec OTF300-03-S3) was used to modify the broadband light. Its peak wavelength is tunable between 1530 nm and 1570 nm. Figure 3(a) shows the spectrum of one of the sensing FBGs relative to the filtered output from the edge filter. In Figure 2(b), the filtered spectrum basically corresponds to the reflected Bragg spectrum of the filter FBG. The laser ring serves to amplify the light intensity of this spectrum. The resulting output spectrum together with the spectrum of the sensing FBG is shown in Figure 3(b). The overlapped regions (hatched areas in Figure 3) loosely illustrate the light energy that will be reflected and transformed into voltage signals by the photodetectors. On receiving a strain wave signal from an impact, the wavelengths of the FBG spectra will shift to and fro horizontally, giving rise to variations of the hatched areas. The voltage outputs from the photodetectors will therefore change corresponding to the strain signal. This forms the basis of light intensity demodulation. The voltage signals were recorded with a 4-channel digital storage scope. Note that the FBG spectra in Figure 3 are obtained by using an unfiltered broadband light and so they appear similar in Figures 3(a) and 3(b). In the actual measuring schemes, the amount of energy reflected (or the hatched areas) will depend on the intensity of the sources. Considering the mechanism of demodulation, the usable demodulation range of the ASE scheme is ~0.5 nm and that of the laser ring is ~0.2 nm. It can be seen that the peak intensity from the laser ring output is much higher than that from the ASE source. With a higher peak intensity and narrower wavelength range, the slope of the edge filter will be steeper, resulting in a more sensitive demodulation with better wavelength resolution. Thus we expect the output from the laser ring scheme to be larger for the same strain disturbance. The sensitivity and accuracy of the measuring system as a whole depends not only on the sensitivity of the demodulation scheme but also on the intrinsic sensitivity of an FBG to the impact stress wave. It is hoped that by employing the above schemes with different output signal strengths and demodulation ranges, the relative importance of the two effects on the overall sensitivity and accuracy can be differentiated.

2.3. Impact Source Locating. To do away with the need for *a priori* knowledge on the wave speed when using the three-sensor-based impact source locating scheme [8, 9], a four-sensor-based algorithm with layout and nomenclature shown in Figure 4 was employed for the aluminum plate. The location of an impact (X, Y) is related to the coordinates (x_i, y_i) of a sensing FBG through the following set of equations:

$$\begin{aligned}
&\sqrt{(X-x_2)^2+(Y-y_2)^2} \\
&\quad=\sqrt{\left(\sqrt{(X-x_1)^2+(Y-y_1)^2}+C\times t_{21}\right)^2}, \\
&\sqrt{(X-x_3)^2+(Y-y_3)^2} \\
&\quad=\sqrt{\left(\sqrt{(X-x_1)^2+(Y-y_1)^2}+C\times t_{31}\right)^2}, \\
&\sqrt{(X-x_4)^2+(Y-y_4)^2} \\
&\quad=\sqrt{\left(\sqrt{(X-x_1)^2+(Y-y_1)^2}+C\times t_{41}\right)^2},
\end{aligned} \tag{1}$$

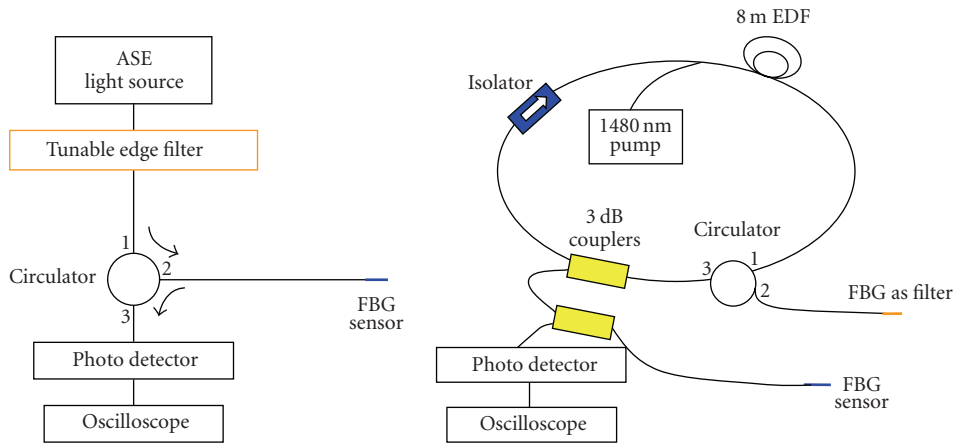

(a) ASE light source scheme (b) Laser ring scheme

FIGURE 2: Two interrogation schemes used to demodulate the wavelength variations in the sensing FBG.

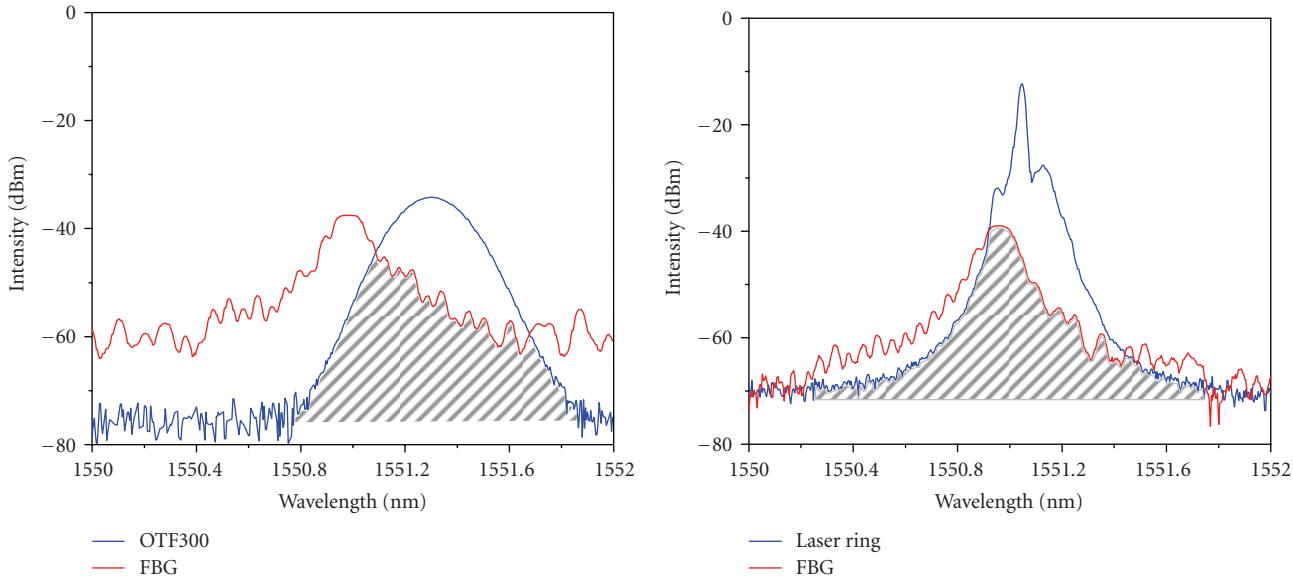

FIGURE 3: Relative spectra between the light source and the sensing FBG for schemes involving (a) an ASE source modified with an edge filter, (b) a laser ring configuration.

where C is the wave speed and t_{ij} is the difference in the time of receiving the wave signal between the sensor i and the sensor j. t_{ij}'s are derived from the oscilloscope recorded signals. Either side of (1) can only take the positive value as the physical meaning of distance.

In the above algorithm, the wave speed C is assumed to be homogeneous at all places and in all directions. Such is the case for the aluminum plate. The material and structural make-up of a wind turbine blade are highly complex and this homogeneous wave speed requirement will certainly be violated. Moreover, with the FBGs deployed near the hub base and the slender aspect ratio of the blade, the distances between impact points with the same x-coordinate but different y-coordinates and a far away FBGs will be similar. It will be difficult to differentiate the y-coordinates from the difference in time-of-flight of the signals. So in the case of the blade we aim at locating the x-coordinate of an impact in this preliminary work. The wave speed was empirically calibrated by knocking on a series of known locations first. Then knocking on a different set of target locations was made. The time-of-flight data, with reference to the signals from the instrumented hammer, were noted and the corresponding x-coordinates were computed from these time data and the average wave speed.

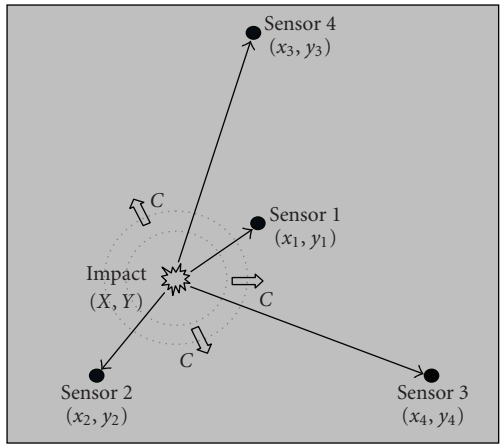

Figure 4: Nomenclature for the 4-sensor algorithm to evaluate the impact location.

3. Results and Discussion

3.1. Detection of an Impact Event. Figure 5 compares the signal received when impacts on the aluminum plate were made at a distance of 60 cm from the sensor with an extremely low energy ($H = 0.1$ mm) and a relatively high energy ($H = 50$ mm) using the two different demodulation schemes. Dotted lines in the figure indicate the first arrival of the impact signal. This time was obtained by first filtering the waveform with a digital band-pass filter with cutoff frequencies of 1 kHz and 100 kHz. A proper length of the leading part of the filtered waveform excluding the impact signal was then chosen to compute the average noise level. The first point where the waveform deviates 20% beyond this average noise level is taken as the first arrival point. With this criterion, the standard deviation of arrival time difference from three identical impact events at a particular impact position was found to be within 2 μsec. in the angular sensitive range of the FBG.

With the same impact energy, the waveforms of the signals obtained from both schemes are similar. For the ASE light source scheme, the signal is heavily masked by background noises. Although a disturbance can be discerned, clear definition of the first arrival of the stress wave is difficult when the impact is from the extremely small height of 0.1 mm (Figure 5(a)). When the impact energy is relatively high, the signal-to-noise ratio is high enough to allow an unambiguous detection of the impact. With the laser ring scheme, the low energy impact can be comfortably detected (Figure 5(b)). With a 1-microstrain disturbance, the signal outputs are 6.6 mV and 623 mV for the ASE and laser ring schemes, respectively. The noise levels of both schemes are roughly the same at 5 mV as the main source of noise is from the photodiode circuitry. Thus the signal-to-noise ratio of the laser ring scheme is approximately 100 times that of the ASE scheme. This high signal strength is a direct consequence of the high intensity light source from the laser ring configuration.

Figure 6 compares the signal received when the impacts on the wind turbine blade were made at $x = 10$ m and 20 m with a momentum roughly equivalent to the impact of a 10 g bird flying at 10 m/s towards the blade. As before, for the same impact condition, the waveforms of the signals from both schemes are basically alike. With the current strength of impact, the signal levels from either schemes allow an unambiguously detection of the occurrence of stress wave disturbance. The signal-to-noise ratio from the ASE scheme (Figure 6(a)) is significantly lower than that from the laser ring scheme (Figure 6(b)) but the initial disturbance signals are clear enough to be defined.

3.2. Impact Source Location. As is evident from (1), accurate determination of the difference in the times of receiving the wave signals between any pair of FBGs is crucial to the accurate evaluation of an impact location. It has been shown that error in the signal receiving time arises due to (i) angular insensitivity of the FBG; (ii) attenuation of signal over distance, and (iii) intrinsic background noises of the optical and electronic circuits [10]. Angular insensitivity results when the impact stress wave fails to cause significant strain variations on the FBG because its incidence is at an oblique angle with the FBG axis. As can be seen in Figure 5, the initially arrived disturbance is very small. Previous work [10] showed that when the point of impact is 20 cm from the FBG and within $\pm 30^\circ$ about the FBG axis, the first arrival of the impact signal was marked with a clearly defined deviation from the background noises. This initial deviation became smaller as the off-axis angle is increased. At an off-axis angle of 60°, the deviation was very small and difficult to discern so that the arrival time was subject to an error upward of 1 μsec. This uncertainty increased rapidly with the off-axis angle and at 75°, the error was likely to be around 10 μsec.This sort of error would be aggravated if the impact occurred at a larger distance from the FBG as signal strength is further degraded by attenuation.

Figures 7(a) and 7(b) compare the experimental impact positions (open circles) on the plate with the locations estimated using the 4-FBGs algorithm (crosses) with the ASE light source and the laser ring scheme, respectively. The corresponding predicted and actual positions are connected with a straight line. For points where discrepancy between the actual and predicted locations is large, only some typical data are shown for clarity of presentation. The layout of the FBGs is also indicated in the figures. The dotted lines in Figures 7(a) and 7(b) define the $\pm 60^\circ$ off-axis boundary of the FBGs and may be treated as the tentative envelop of angular sensitivity limits. The areas bounded by these dotted lines represent regions which are within the $\pm 60^\circ$ off-axis boundary of all four FBGs. It can be seen that all the favorably correlated predicted-actual position pairs do lie within or close to the dotted boundary, suggesting that angular sensitivity of the FBG is a necessary requirement for accurate prediction. Within the dotted line bound regions, significant discrepancies can still occur. Examples for the latter can be found within the triangle near the top and the quadrilateral near the bottom. Incidentally, these two

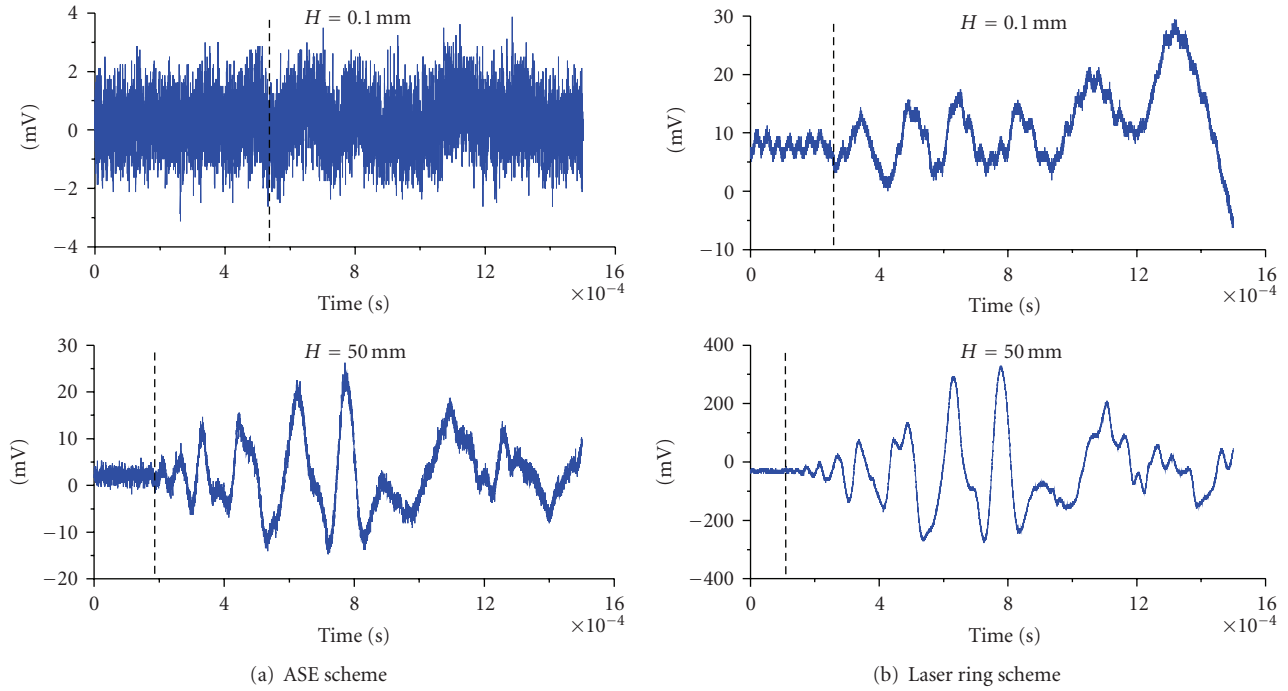

Figure 5: Impact signals obtained on the aluminum plate using (a) the ASE light source and (b) the laser ring scheme. (Dotted lines indicate the signal first arrival time).

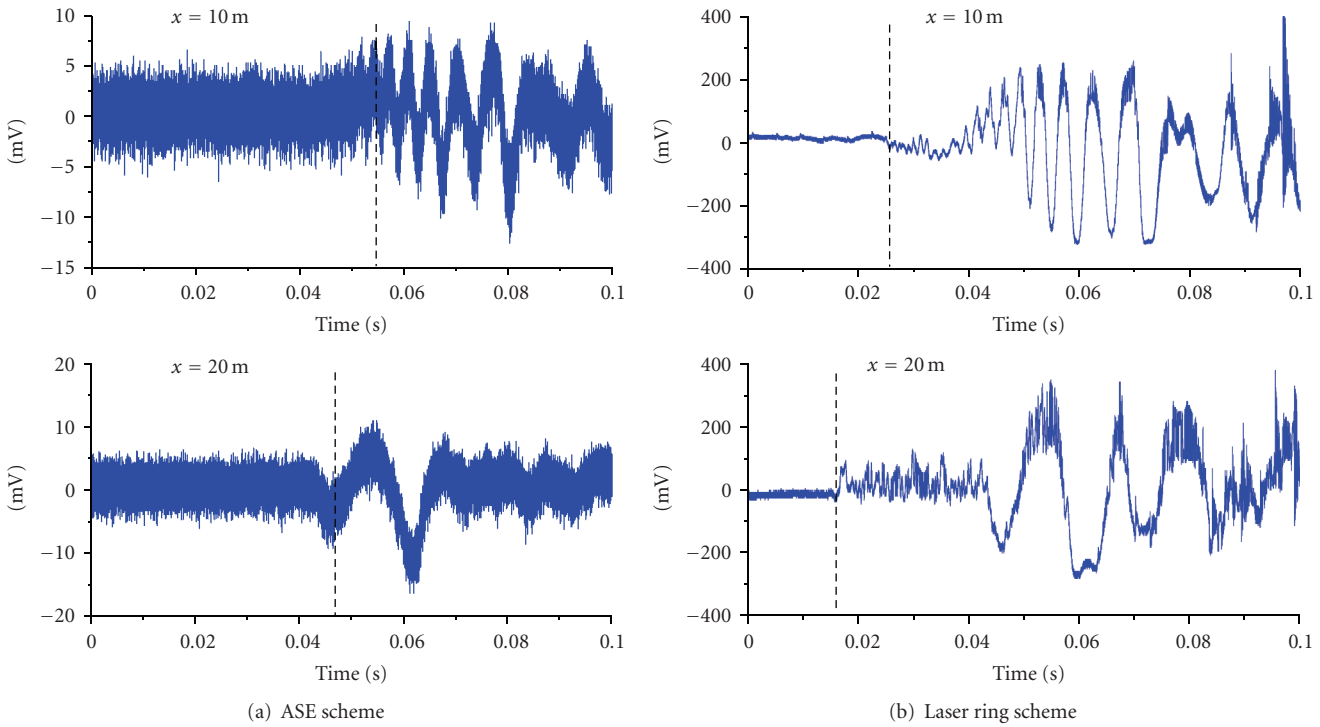

Figure 6: Impact Signals obtained from the wind turbine blade using (a) the ASE light source and (b) the laser ring scheme. (Dotted lines indicate the signal first arrival time).

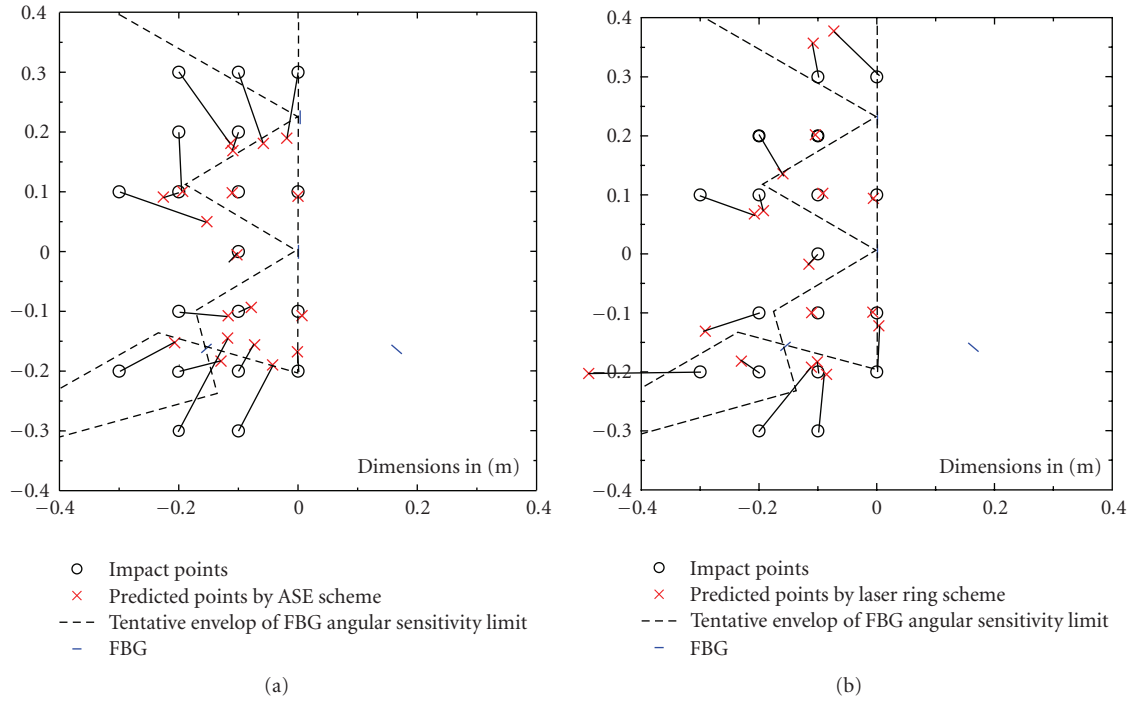

Figure 7: Comparison of the actual and calculated impact locations on the aluminum plate using (a) the ASE light source scheme and (b) the laser ring scheme.

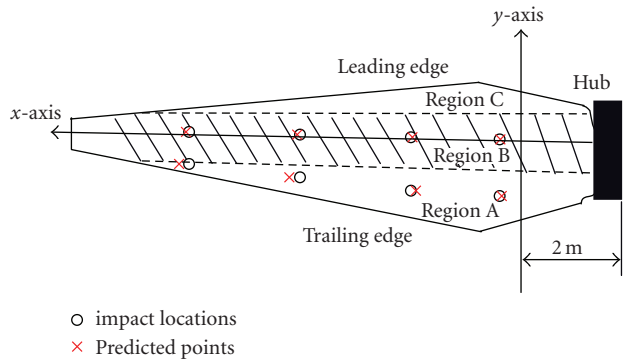

Figure 8: Comparison of the x-coordinates of the experimental impact and predicted locations for Regions A and B on the wind turbine blade.

regions lie far away from one or more of the FBGs. As a result the angular insensitivity of the FBGs concerned is aggravated by signal attenuation and one or more of the t_{ij}'s in (1) will be highly erroneous, leading to an inaccurate prediction of the impact position. If we compare the corresponding points in Figures 7(a) and 7(b), it can be seen that the prediction error based on the laser ring scheme is in general smaller than that on the ASE scheme. This is reasonable as the former has a higher intensity source and the problems of signal attenuation and background noise will be alleviated. However, the fact that the laser ring scheme is only marginally better suggests that the bottleneck of location accuracy is on the angular insensitivity of an FBG. The underlying cause of angular insensitivity is rooted from the way an impact stress wave interacts with an FBG. This fact cannot be modified with a more intense light source and/or steeper filter slope. Hence, to improve the prediction accuracy, other ways have to be sought. A possible method is to use an FBG rosette involving two or three FBGs connected in series at an angle to one another. Preliminary results using FBG rosettes are compared with the above results at two impact positions where the angular insensitivity effect contributed heavily to the location errors (Table 1). The FBG rosettes were made from two FBGs at right angle to each other. For impact at $(-0.2, 0)$, both the ASE and laser ring systems with standalone FBGs failed to give convergent solution while the ASE system with FBG rosettes predicted to within 5 cm of the impact position. For impact at $(-0.2, 0.2)$, the distance between the predicted and the actual impact positions is 3.3 cm for the rosette system. This is significantly better than the 7.6 cm and 10 cm, respectively, for the laser ring and ASE systems with standalone FBGs.

For practical large-scale structures, the intense light source from the laser ring scheme will still be advantageous as signal attenuation will be serious in these cases. Also, with a large structure, the number of deployed sensors may have to be increased. With its high intensity, it is possible to use one laser ring to feed a larger number of FBG sensors, thus reducing the overall equipment cost.

For the ASE scheme (Figure 7(a)), most of the predicted locations tend to locate at the right-hand-side of the actual impact point. The reason of this may be attributed to the nonlinearity of the edge filter and the fact that it is not possible to get exactly the same Bragg spectra for the four

Table 1: Comparison of prediction accuracy among systems using single FBG and FBG rosette.

Impact Locations	Predicted locations		
(units in m.)	ASE System	Ring Laser System	ASE System with FBG Rosette
(−0.2, 0)	no convergent solution	no convergent solution	(−0.164, −0.036)
(−0.2, 0.2)	(−0.193, 0.101)	(−0.159, 0.136)	(−0.225, 0.222)

sensor FBGs. Thus sensitivities of the FBGs to strain wave will be slightly different. A particular FBG may be slightly less sensitive (or more sensitive) and shift the predicted positions towards one side. With the much increased sensitivity of the laser ring scheme, such slight discrepancies may be overridden. In fact, for the laser ring scheme (Figure 7(b)), the deviation to the right or left is more balanced.

In the case of the wind turbine blade, calibration showed that the wave velocities in Regions A and B are fairly constant and equal to 370 ± 21 m/s and 1278 ± 31 m/s, respectively. Calibration in Region C gave random wave speeds, presumably due to the interaction of the stress wave with the complex material composition as well as the irregular boundary geometry. With the wave speed data for Regions A and B, the x-coordinates of the impact locations can be evaluates when hammer knockingd are made at different positions along the blade in these two regions. Figure 8 shows the predicted locations agreed reasonably well with the impact locations. It should be pointed out that an underlying assumption in the current prediction is that the region of knocking is known in advance. Previous work suggested that the region of impact may be identified by the characteristic waveform shapes [15]. Another notable point is that the current prediction does not provide information about the y-coordinates of the impact. In practice, knowing the region and the x-coordinates of a severe impact should be helpful enough to pinpoint the location for more detailed nondestructive examination to ensure structural integrity.

4. Conclusions

An impact monitoring system using fiber Bragg grating sensors has been established. With a laser ring scheme for FBG interrogation, an excellent signal-to-noise ratio is obtained that enables both extremely low energy and higher energy impacts to be detected with ease. The scheme with an ASE light source offered a lower signal strength and is good only for higher energy impacts. With FBGs deployed near the base hub, both schemes are able to detect the occurrence of an impact equivalent to a small bird striking even at the far end tip on a wind turbine blade. In an aluminum plate with homogeneous wave speed which is not known beforehand, location of impact positions is possible with a 4-FBG array. In this case, the laser ring scheme only performed marginally better than the ASE scheme, suggesting that the bottleneck of impact source location accuracy is on the limitation of the angular insensitivity of an FBG. For the wind turbine blade, with precalibrated wave speeds, the longitudinal coordinate of an impact can be located reasonably well in the box beam reinforced region and the trailing edge region. Impact source location in the leading edge region was not successful as the wave speed varied with positions in this region.

Acknowledgments

This work was carried out with support of the National Science Council projects (NSC96-2628-E-002-223-MY3). The authors indebted to Taiwan Power Research Institute for some of the equipment support.

References

[1] Y. J. Rao, "Recent progress in applications of in-fibre Bragg grating sensors," *Optics and Lasers in Engineering*, vol. 31, no. 4, pp. 297–324, 1999.

[2] F. G. Tomasel and P. A. A. Laura, "Assessing the healing of mechanical structures through changes in their vibrational characteristics as detected by fiber optic Bragg gratings," *Journal of Sound and Vibration*, vol. 253, no. 2, pp. 523–527, 2002.

[3] J. S. Leng and A. Asundi, "Non-destructive evaluation of smart materials by using extrinsic Fabry-Perot interferometric and fiber Bragg grating sensors," *NDT and E International*, vol. 35, no. 4, pp. 273–276, 2002.

[4] J. Leng and A. Asundi, "Structural health monitoring of smart composite materials by using EFPI and FBG sensors," *Sensors and Actuators A*, vol. 103, no. 3, pp. 330–340, 2003.

[5] H.-Y. Ling, K.-T. Lau, L. Cheng, and W. Jin, "Fibre optic sensors for delamination identification in composite beams using a genetic algorithm," *Smart Materials and Structures*, vol. 14, no. 1, pp. 287–295, 2005.

[6] P. T. Coverley and W. J. Staszewski, "Impact damage location in composite structures using optimized sensor triangulation procedure," *Smart Materials and Structures*, vol. 12, no. 5, pp. 795–803, 2003.

[7] M. Meo, G. Zumpano, M. Piggott, and G. Marengo, "Impact identification on a sandwich plate from wave propagation responses," *Composite Structures*, vol. 71, no. 3-4, pp. 302–306, 2005.

[8] A. Tobias, "Acoustic-emission source location in two dimensions by an array of three sensors," *Non-Destructive Testing*, vol. 9, no. 1, pp. 9–12, 1976.

[9] H. A. Canistraro and E. H. Jordan, "Projectile-impact-location determination: an acoustic triangulation method," *Measurement Science and Technology*, vol. 7, no. 12, pp. 1755–1760, 1996.

[10] B. L. Chen and C. S. Shin, "Fiber Bragg gratings array for structural health monitoring," *Materials and Manufacturing Processeses*, vol. 25, no. 1-4, 2010.

[11] L. Zhang, R. Fallon, L. A. Everall, J. A. R. Williams, and I. Bennion, "Large-dynamic-range and high-resolution from a strain sensing system using long-period grating interrogating FBG strain sensor," in *Proceedings of the 24th European Conference on Optical Communication (ECOC '98)*, vol. 1, pp. 609–610, Madrid, Spain, September 1998.

[12] R. W. Fallon, L. Zhang, A. Gloag, and I. Bennion, "Multiplexed identical broad-band-chirped grating interrogation system for

large-strain sensing applications," *IEEE Photonics Technology Letters*, vol. 9, no. 12, pp. 1616–1618, 1997.

[13] R. W. Fallon, L. Zhang, A. Gloag, and I. Bennion, "Identical broadband chirped grating interrogation technique for temperature and strain sensing," *Electronics Letters*, vol. 33, no. 8, pp. 705–707, 1997.

[14] C. S. Shin, B. L. Chen, and C. C. Chiang, "A dynamic strain measurement system using fiber grating sensors and its application in structural health monitoring," in *Proceedings of the World Forum on Smart Materials and Smart Structures Technology (SMSST '07)*, p. 335, Nanjing, China, May 2007.

[15] C. S. Shin, B. L. Chen, J. R. Cheng, and S. K. Liaw, "Impact response of a wind turbine blade measured by distributed FBG sensors," *Materials and Manufacturing Processes*, vol. 25, no. 1-4, 2010.